HOKKAIDO UNIVERSITY

| | |
|---|---|
| Title | Numerical simulation of an open sorption thermal energy storage system using composite sorbents built into a honeycomb structure |
| Author(s) | Liu, Hongzhi; Nagano, Katsunori |
| Citation | International Journal of Heat and Mass Transfer, 78, 648-661<br>https://doi.org/10.1016/j.ijheatmasstransfer.2014.07.034 |
| Issue Date | 2014-11 |
| Doc URL | https://hdl.handle.net/2115/57488 |
| Type | journal article |
| File Information | Numerical simulation of an open sorption thermal.pdf |

Hokkaido University Collection of Scholarly and Academic Papers : HUSCAP

# Numerical simulation of an open sorption thermal energy storage system using composite sorbents built into a honeycomb structure

Hongzhi **Liu***, Katsunori **Nagano**

Environmental System Research Laboratory, Hokkaido University, N13-W8 Sapporo 060-8628, Japan

## Abstract

A new composite mesoporous honeycomb material was developed to be a thermal energy storage medium that can contact the functional fluid directly. In our previous study, this honeycombed composite material acted as a promising sorption thermal energy storage medium in an open system, exhibiting a lower regeneration temperature as 80°C, high volumetric heat storage density, and high stability. In the present study, a one-dimensional transient model was used to predict both the heat storage process (desorption process) and heat release process (sorption process) occurring in the open sorption thermal energy storage unit. Our model was validated using the experimental results obtained in our previous experiments, and a close agreement was observed for the sorption process. Some discrepancy was observed in the desorption process, but it has been explained. The sorption and desorption processes were simulated repeatedly for 20 cycles, whose result was also compared with the experimental result. The operating parameters of the open thermal energy storage system were evaluated to determine its operation performance. Finally, our open thermal energy storage system was assumed to be incorporated into a paint-drying system, within which the heat storage unit is regenerated for ten hours by the exhaust heat produced by a blower in the daytime and releases its stored heat during the nighttime for 14 hours. The simulation result shows that almost 51.3% of the blower's waste heat can be reutilized if the proposed thermal energy storage system is incorporated.

**Keywords:** Composite mesoporous material; Open sorption thermal energy storage; Heat and mass transfer; Linear driving force model (LDF)

## 1. Introduction

Thermal energy storage technology has the potential to meet society's need for more efficient, environmentally friendly energy use in a variety of sectors, and it appears to be the only viable solution to overcome the mismatch between the supply and demand of thermal energy [1]. Effective storage of thermal energy could reduce both fossil energy demand and carbon dioxide emissions. A composite thermal energy storage material with low heat loss and high heat storage density for the storage of low-temperature industrial waste heat (80°C) was developed in our previous work [2]. The composite material based on a natural mesoporous stone (Wakkanai siliceous shale (WSS)), whose main composition is $SiO_2$, was built into a honeycomb shape, and it was installed in an open sorption thermal energy storage system, with which it can be regenerated by hot air at 80-120°C. Compared to the traditional sensible heat storage and latent heat storage materials, the developed composite material exhibits low heat loss as it can be stored at ambient temperatures as long as it is separated with the functional gas (water vapor) [3]. Another advantage of this material would be the low cost, due to the low price of natural mudstone WSS and cheap $CaCl_2$. Furthermore, from the viewpoint of thermal energy storage density, this material can compete with the traditional sensible heat storage and phase change materials from Fig.16 in [2].

So far, there are few research studies about open sorption thermal energy storage system. Wu and Zhu and Wu et al. [4, 5] developed an open-type thermal energy storage setup with 40 kg composite sorbent pellets (silica gel filled with $CaCl_2$). Moreover, they also reported a three-dimensional numerical model [6] to determine the dynamic characteristics of composite sorbents and to calculate the specific capacity and coefficient of performance (COP) of the open system. According to their results, the developed system showed high thermal energy storage density and can be regenerated at low temperature (<100ºC). Ostrovskii et al. [7, 8] have proposed a non-stationary model to describe water sorption in a flow adsorber with a

fixed bed of selective water sorbents (SWSs) (calcium chloride in a porous matrix) at pressures of 7 atm and 1 atm, respectively. An analytical expression for the sorption rate constant as a function of the moisture content of the sorbent is proposed that takes into account the monotonic decrease in this constant with an increase in the amount of water sorbed. Unfortunately, both of the two open systems described above keep the functional fluid flow through the inter particles of their composite materials without an individual flow passage for fluid, which would cause a high pressure drop. Moreover, a heat exchanger is needed to improve the heat exchange between the air and the composite material [4].

In fact, the heat and mass transfer between the flowing air and the composite material occurring in this open system is very similar with the heat and mass transport which happens in solid desiccant systems. Many researchers have simulated heat and moisture transfer in solid desiccant systems, in which the coupled heat and moisture transfer is of great importance to the system performance [9]. Among these models, Charoensupaya et al. [10] proposed a one-dimensional heat and mass transfer model to analyze an open-cycle desiccant cooling system based on a hypothetical isotherm equation. Then a one-dimensional transient model has been established by Zheng et al. [11, 12], with which the optimum rotational speed for air dehumidification was determined. Zhang et al. [13] also proposed a one-dimensional theoretical model based on the size and structure of the channel in their desiccant wheel for wheel design optimization. However, the actual transfer process occurring in the desiccant wheel cannot be reflected by these models, as the solid side resistance (heat conduction and mass diffusion within solid side) were ignored. Realizing the above problem, many researchers have developed models by taking both gas and solid side resistances into account, including Majumdar [14], Ge et.al [15], Gao et al. [16], Zhang and Niu [9, 17], Yamaguchi et al. [18] etc. By considering both the gas and solid side resistance, the precisions of simulation models can be greatly improved [15].

Compared to the common solid desiccant system, the operating relative humidity range of our system is much larger (2%-95%) during the sorption process. In this case, the formation of crystalline hydrate needs to be considered. Compared to the traditional solid desiccant materials, the presence of hydrates or salt solution in the matrix's pores, however, can significantly change the sorbent capacity and also induce qualitatively new phenomena [8], which increases the difficulty of simulating the sorption and desorption processes of composite materials. In order to increase the precision of simulation results, Ge et al. [15] used a one-dimensional model to predict the performance of silica gel haloid compound desiccant wheel by considering both the gas and solid side resistances. For the solid side resistance, both pore diffusion and surface diffusion have been considered.

The objective of our current research is to simulate the processes of sorption (heat release) and desorption (heat storage) within this thermal energy storage unit quickly and accurately by numerical simulation. Such a simulation can be used to predict the temperature distribution of the thermal energy storage unit and the flowing air, quickly evaluate the performance of the thermal energy storage system, and optimize the air conditions for practical applications. Moreover, the air condition and the necessary volume of this composite thermal energy storage unit are expected to be designed and calculated by this model according to the requirement of a certain application.

**Nomenclature**

Abbreviation

| | |
|---|---|
| COP | coefficient of performance; |
| LDF | linear driving force model; |
| SWSs | selective water sorbents; |
| WSS | Wakkanai siliceous shale; |

Symbols

| | |
|---|---|
| $B_{ih}$ | heat transfer Biot number (−); |
| $B_{im}$ | mass transfer Biot number (−); |
| $C_p$ | specific heat (J/ (kg·K)); |
| $d_a$ | Hydraulic diameter of the air channel (m); |
| $D_m$ | molecular diffusion coefficient ($m^2$/s); |
| $D_K$ | Knudsen diffusion coefficient ($m^2$/s); |
| $D_P$ | overall pore diffusivity ($m^2$/s); |
| $D_s$ | coefficient of surface diffusion ($m^2$/s); |
| $D_{s,0}$ | constant for surface diffusivity calculation ($m^2$/s); |
| $D_{eff}$ | Apparent pore diffusion coefficient based on gas side ($m^2$/s); |
| $f_a$ | air flow rate ($m^3$/h); |
| $f$ | air flow rate, $f_a$ /3600 ($m^3$/s); |
| $h$ | heat transfer coefficient (W/($m^2$·K)); |
| $h_m$ | convective mass transfer coefficient (m/s); |
| $k_a$ | air side mass transfer coefficient based on solid side (m/s); |
| $k_s$ | solid side mass transfer coefficient (m/s); |
| $K$ | overall mass transfer coefficient (m/s); |
| $L$ | length of the unit (m); |

$Le$ Lewis number (−);

$M$ molecular weight (g/mol);

$m_{s,dry}$ mass of the dry composite material (kg);

$Nu$ Nusselt number (−);

$P_0$ pressure in atmospheres (Pa);

$Q_V$ volumetric heat storage density (J/m$^3$);

$Q$ heat amount (J);

$r_p$ pore's radius (m);

$RH$ relative humidity of air (%);

$t$ time (s);

$T$ temperature (ºC);

$u$ velocity (m/s);

$V$ volume of the honeycomb heat storage unit(m$^3$);

$W_V$ volumetric heat transfer rate of the heat storage unit (W/m$^3$);

$x$ absolute humidity (g/kg$_{DA}$);

$X_a$ mass flow of water vapor in the air (g/s);

$z$ direction of length (m);

Greek letters

α sorption equilibrium constant (g/g);

Δ$H$ sorption heat (J/kg);

Δ$T$ inlet and outlet temperature difference (ºC);

Δ$t$ time interval (s);

Δ$\omega$ change of the sorption amount ($g_{H2O}/g_{sample}$);

$\delta_a$ The thickness of air, equals to $d_a/4$ (m);

$\delta_s$ thickness (m);

| | |
|---|---|
| $\varepsilon$ | coefficient of heat extraction performance during the heat release process (−); |
| $\varepsilon_s$ | Porosity of the composite porous material (−); |
| $\eta$ | heat recovery rate (−); |
| $\lambda$ | effective thermal conductivity (W/(m·K)); |
| $\rho$ | bulk density (kg/m$^3$); |
| $\tau_p$ | tortuosity of real pores (−); |
| $\tau_s$ | tortuosity factor for surface diffusion (−); |
| $\omega$ | sorption amount ($g_{H2O}/g_{sample}$); |
| $\omega_s$ | sorption amount on the gas and solid surface ($g_{H2O}/g_{sample}$); |

Subscripts

| | |
|---|---|
| a | air; |
| $CaCl_2$ | calcium chloride; |
| desor | desorption process; |
| dry | dry state of composite material; |
| e | equilibrium state; |
| eff | effective; |
| $H_2O$ | water or water vapor; |
| max | maximum; |
| in | inlet; |
| out | outlet; |
| s | solid material; |
| sor | sorption process; |
| 0 | initial condition; |

## 2. Mathematical model

For a thermal energy storage system, heat storage process and heat release process are included. An open sorption thermal energy storage experimental setup was built as described in our previous study [2]. In the heat storage (heat charging or endothermic) process, hot air is used to regenerate the material, during which the water vapor bonded to the material is discharged to the ambient environment and the heat is stored. In the heat release (heat discharging or exothermic) mode, high-humidity air flows through the system to recover the exothermic heat due to the sorption of the water vapor. A composite mesoporous honeycomb thermal energy storage unit was the key component in that open sorption thermal energy storage system operated under atmospheric pressure of 1 atm. The honeycomb structure can assure high heat and mass transfer contact area with a low pressure drop. The pressure drop is less than 15 Pa at a flow rate of 10 $m^3$/h when the dimension of the unit is 10 cm × 10 cm × 10 cm. The thermal energy storage unit was made by impregnating calcium chloride ($CaCl_2$) into the mesopores of WSS honeycomb unit. The schematic of the honeycomb structure and a cross section of one channel used in the model are shown in Fig. 1(a), in which the length is illustrated as *L* and size of each channel can also be checked. Three samples with different $CaCl_2$ contents were made, and were short for WSS + 2.2 wt % $CaCl_2$, WSS + 13.0 wt% $CaCl_2$, WSS + 22.4 wt% $CaCl_2$, respectively. The physical properties of these composite mesoporous materials including pore volume distributions, porosity and true density.etc can be checked in Fig. 2 and Table 1 in reference [2].

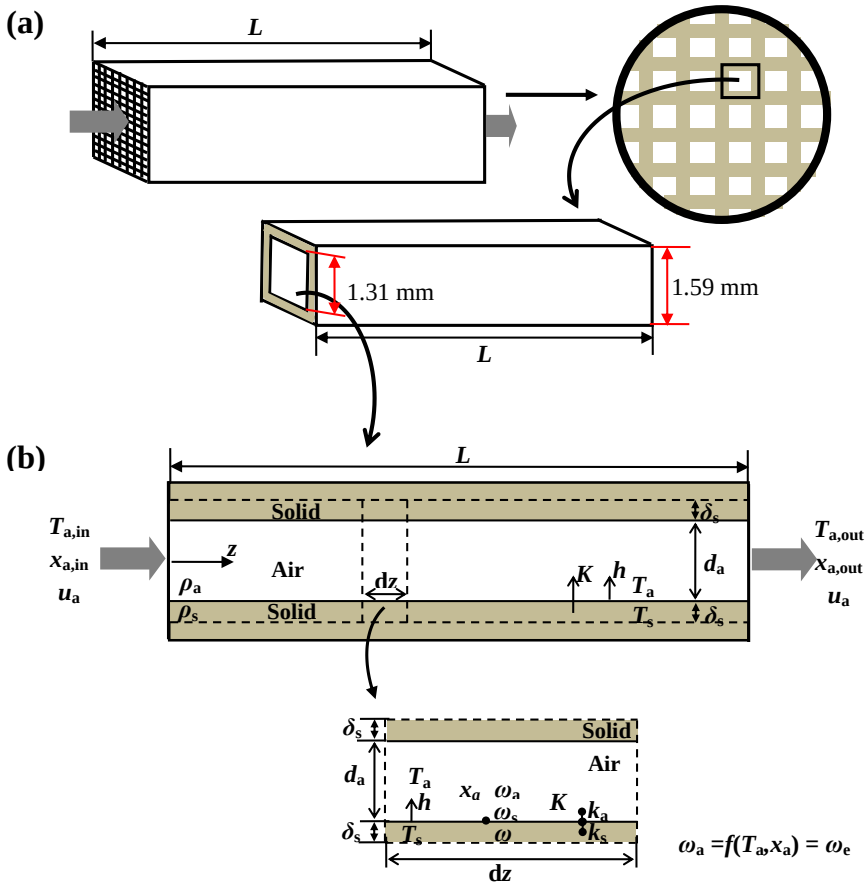


Fig. 1 The one-dimensional transient model illustration

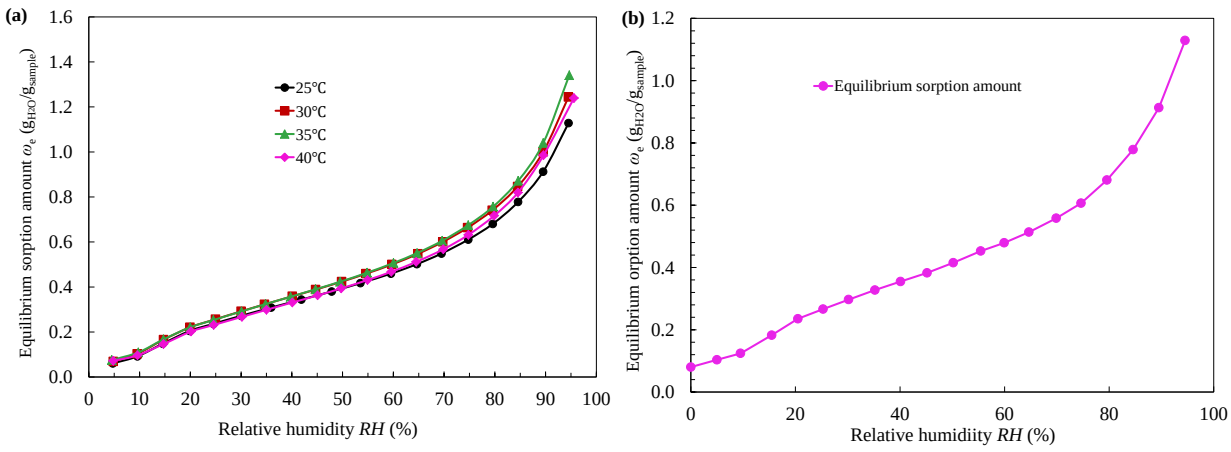


Fig. 2 (a) Equilibrium sorption amount at different temperatures for the WSS +22.4 $CaCl_2$; (b) equilibrium sorption fitting lines used in simulation for the WSS +22.4 $CaCl_2$

The performance the thermal energy storage unit is modeled by just tracking the air and solid condition in one single channel. A one-dimensional transient model, illustrated in Fig.

1(b), was proposed to predict the temperature of the composite material and the temperature and humidity of the flowing moist/hot air and to evaluate the performance of the thermal energy storage medium.

**Table 1** Air states and initial conditions of both air and composite material in sorption/desorption process

| | Process | Sorption | Desorption |
|---|---|---|---|
| Inlet air condition | Inlet air flow rate $f_a$ ($m^3$/h) | 3.0 | 3.8 |
| | Inlet air temperature $T_a$ (°C) | 25 | 80 |
| | Inlet air relative humidity *RH* (%) | 95 | 3 |
| Initial condition | Air temperature $T_a$ (°C) | 25 | 25 (lnlet)<br>35 (outlet) |
| | Air relative humidity *RH* (%) | 3.0 | 95.4 (lnlet)<br>36.6 (outlet) |
| | Composite material's temperature $T_s$ (°C) | 25 | 30 |
| Repetition test | Inlet air flow rate $f_a$ ($m^3$/h) | 2.0 | 2.8 |
| | Inlet air temperature $T_a$ (°C) | 25 | 80 |
| | Inlet air relative humidity *RH* (%) | 95 | 3 |

2.1 Heat and mass transfer analysis

As humid/hot air enters the channel of the honeycomb unit, a fraction of the water vapor is sorbed/desorbed by the composite material. The sorption/desorption process is accompanied by a release/absorption of heat, creating a strong coupling between heat and mass transfer [19]. Generally, the water vapor transfers from the air to the pores of the composite material mainly in two steps. First, water molecules are transported from the air to the surface of the composite material due to convective mass transfer, which is called gas side mass transfer. In the next step, the water vapor transfers from the surface of the composite material to the inter particle pores and then to the intra particle pores. Mass diffusion inside the solid involves multiple mechanisms – molecular diffusion, Knudsen diffusion, and surface diffusion [20] – occur in the porous material. Water molecules in the vapor phase diffuse from the surface of

the composite solid layer to the surface of the particles through molecular and Knudsen diffusion in the inter-particle pores. The sorbed water molecules then diffuse from the surface of the particles into the intra-particle pores through surface diffusion, and water vapor molecules in the intra-particle pores diffuse through molecular and Knudsen diffusion [21]. The mass transfer is also accompanied by heat transfer. Heat transfer between the flowing air and the channel of the composite material occurs primarily due to the convective heat transfer along the surface of each channel. The heat transfer inside the solid layer would be the heat conduction between the solid particles.

2.1.1 Heat transfer Biot number

The heat transfer Biot number $B_{ih}$ is calculated to determine whether thermal conduction on the solid side is relevant, which is defined as follows:

$$B_{ih} = \frac{h\delta_{\mathrm{s}}}{\lambda_{\mathrm{s}}} \tag{1}$$

The convective heat transfer coefficient is estimated from the Nusselt number $Nu$ for developed laminar flow in a square channel, considering constant and uniform temperature at the interface as 2.89.

$$h = Nu\frac{\lambda_a}{d_{\mathrm{a}}} \tag{2}$$

The effective thermal conductivity is considered to be related to the amount of water sorbed.

$$\lambda_{\mathrm{s}} = \lambda_{\mathrm{s,dry}} + \lambda_{\mathrm{H_2O}}\omega \tag{3}$$

Thickness of the solid layer $\delta_{\mathrm{s}}$ of 0.14 mm and thermal conductivity of the dry material $\lambda_{\mathrm{s,dry}}$ of 0.2 W/(m·K) were used for the Biot number $B_{ih}$ calculation. The calculated maximum heat transfer Biot number $B_{ih}$ for our system is 0.035; therefore, the solid inside heat conduction resistance can be ignored due to the small heat transfer Biot number ($B_{ih} < 0.1$).

2.1.2 Mass transfer Biot number

Similar to the heat transfer Biot number $B_{ih}$, the mass transfer Biot number $B_{im}$ is introduced to determine the dominant mass transfer resistance [22]. $B_{im}$ represents the relative importance of the intraparticle diffusion resistance and fluid to particle mass transfer resistance, which is defined as follows [20]:

$$B_{im} = \frac{h_m \delta_s}{D_{eff}} \tag{4}$$

The solid inside mass transfer resistance can be ignored if the mass transfer Biot number is small ($B_{im}$ <0.1), similar to the requirement for ignoring heat conduction for small heat transfer Biot numbers [21].

The gas side mass transfer coefficient $h_m$ is estimated after the calculation of the convective heat transfer coefficient. When both heat and mass transfer occur simultaneously, the mass and heat transfer coefficients are related by the Lewis equation [23]:

$$h_m = \frac{h}{\rho_a C_{p,a} Le} \tag{5}$$

The molecular diffusion coefficient $D_m$ is calculated based on the kinetic theory of gases, and for a water vapor-air mixture, it is given by [14, 17]:

$$D_m = 1.758 \times 10^{-4} \frac{(T_s + 273.15)^{1.685}}{P_0} \tag{6}$$

In the above equation, $P_0$ is the pressure in atmospheres (Pa). The calculated molecular diffusion coefficient is on an order of $1.0 \times 10^{-5}$ $m^2/s$.

Knudsen diffusion $D_K$ is significant at low pressure and small pore diameter, and it depends on the radius of the pore $r_p$ and the material's temperature $T_s$ [24]:

$$D_K = 97 r_p ((T_s + 273.15)/M)^{1/2} \tag{7}$$

The average pore diameter of WSS + 22.4 wt% $CaCl_2$ is about 6 nm. When temperature is 25ºC, the calculated Knudsen diffusion coefficient $D_K$ is $1.18 \times 10^{-6}$ $m^2/s$.

The overall pore diffusivity $D_P$ inside the solid pores can be obtained from Bosanquit's equation [20]:

$$1/D_P = 1/D_m + 1/D_K \tag{8}$$

Surface diffusion $D_s$, the transport of sorbed molecules on the pore surface, can be expressed as a function of temperature [25]:

$$D_s = D_{s,0} \exp(-0.974\times10^{-3} \frac{\Delta H}{T_s + 273.15}) \tag{9}$$

$D_{s,0}$ is a constant for surface diffusion calculation, which has a constant value of $1.6\times10^{-6}$ $m^2/s$. The calculated surface diffusion coefficient is in the order of $1.0 \times 10^{-10}$ $m^2/s$.

The pore diffusion and the surface diffusion are considered to occur in parallel [18]. The apparent pore diffusion coefficient $D_{\text{eff}}$ was defined by taking the water vapor content gradient as the driving force of diffusion [20].

$$D_{\text{eff}} = \frac{\varepsilon_s}{\tau_p} D_p + \frac{\rho_s}{\rho_a} \frac{D_s}{\tau_s} \alpha \tag{10}$$

In the above equation, $\alpha$ reflects the local slope of the equilibrium sorption amount to the absolute humidity, and it can be represented as: $d\omega_e / dx_a$. $\tau_p$ accounts for the increase in diffusional length due to the tortuosity of real pores, which is set as 3 in this study assuming the random pore direction [20]. $\tau_s$ is the tortuosity factor for surface diffusion, which accounts for the increase in diffusion resistance in real pores compared with theoretically smooth surface [22], which is set the same as $\tau_p$ in this calculation. In this study, the overall pore diffusivity $D_P$ is in the order of $1.0 \times 10^{-7}$ $m^2/s$, whiles the effective surface diffusion coefficient, the latter term of Eq. (10), based on the pore diffusion is in the order of $1.0 \times 10^{-5}$ $m^2/s$. Therefore, the surface diffusion is dominant compared to the pore diffusion in the composite material, and the apparent pore diffusion coefficient can be changed to the following equation:

$$D_{\text{eff}} = \frac{\rho_{\text{s}}}{\rho_{\text{a}}} \frac{D_s}{\tau_{\text{s}}} \alpha \tag{11}$$

The calculated $B_{im}$ is about 0.3 when the calculating temperature is 25ºC, indicating that neither the gas side mass transfer resistance nor the mass diffusion inside the composite material can be ignored.

## 2.2 Governing equations

### 2.2.1 Assumptions

The governing equations describing the mass and energy balances are developed based on the following assumptions:

(1) The structure and composition of the honeycomb unit are assumed homogeneous.

(2) All the channels are considered identical in the calculations.

(3) The pressure and temperature of the air are assumed to be constant in the direction perpendicular to air flow, and the air's velocity is assumed to be constant along the thickness of the air layer and throughout the sorption/desorption process. Pressure, temperature, and the amount of sorbed water vapor are assumed to be constant along the thickness of the composite material.

(4) The flowing air is incompressible and laminar because the hydraulic diameter of each cell is 1.31 mm, and a typical Reynolds number is in the order of 100.

(5) The heat conduction and water vapor diffusion in the air along the length of the material is negligible.

(6) Convective heat transfer is used to describe the interfacial heat transfer between the solid composite material and the airflow.

(7) The specific heat and density of the dry composite material are constant.

(8) The impregnation of hydroscopic salt is assumed not to affect the sorption process such as the diffusion of water vapor into solid salt or through the liquid film of $CaCl_2 \cdot nH_2O$.

(9) The LDF model is adopted to predict the sorption rate by considering both the gas side and the solid side mass transfer resistances.

2.2.2 Conservation equations

The mass conservation equation for water vapor in the air can be written as follows:

$$\rho_{\mathrm{a}} \frac{\partial x_{\mathrm{a}}}{\partial t} + \rho_{\mathrm{a}} u_{\mathrm{a}} \frac{\partial x_{\mathrm{a}}}{\partial z} = -\rho_{\mathrm{s}} \frac{\partial \omega}{\partial t} \frac{\delta_{\mathrm{s}}}{\delta_{\mathrm{a}}} \tag{12}$$

The moisture balance of the composite material can be written using the Linear driving force (LDF) model:

$$\frac{\partial \omega}{\partial t} = \frac{K}{\delta_{\mathrm{s}}} (\omega_{\mathrm{e}} - \omega) \tag{13}$$

The energy conservation equation for the air is as follows:

$$\rho_{\mathrm{a}} C_{p,\mathrm{a}} \frac{\partial T_{\mathrm{a}}}{\partial t} + \rho_{\mathrm{a}} u_{\mathrm{a}} C_{p,\mathrm{a}} \frac{\partial T_{\mathrm{a}}}{\partial z} = \frac{h}{\delta_{\mathrm{a}}} (T_{\mathrm{s}} - T_{\mathrm{a}}) \tag{14}$$

The energy conservation equation for the composite solid is as follows:

$$\rho_{\mathrm{s}} C_{p,\mathrm{s}} \frac{\partial T_{\mathrm{s}}}{\partial t} = \frac{h}{\delta_{\mathrm{s}}} (T_{\mathrm{a}} - T_{\mathrm{s}}) + \rho_{\mathrm{s}} \frac{\partial \omega}{\partial t} (\Delta H) \tag{15}$$

The specific heat of the composite material is considered to be related to the amount of water vapor sorbed according to Eq. (16):

$$C_{p,\mathrm{s}} = C_{p,\mathrm{s,dry}} + C_{p,\mathrm{H_2O}} \omega \tag{16}$$

2.2.3 Boundary and initial conditions

(1) Boundary conditions

Inlet condition: Uniform distributions of $T_{\mathrm{a}}$ and $x_{\mathrm{a}}$ are assumed as the inlet air condition.

$$x_{\mathrm{a}} = x_{\mathrm{a,in}}, T_{\mathrm{a}} = T_{\mathrm{a,in}} \qquad \text{at } z = 0 \qquad (17a)$$

Outlet condition: The adiabatic and impermeable condition of the outlet of the thermal energy storage unit was set. It is assumed that the absolute humidity gradient and temperature gradient of the air vanished at the outlet of the channel.

$$\frac{\partial x_{\mathrm{a}}}{\partial z} = 0, \frac{\partial T_{\mathrm{a}}}{\partial z} = 0 \qquad \text{at } z = L \qquad (17b)$$

(2) Initial condition

The initial sorption amount of the composite material of one process is equal to the final sorption amount of the reverse process. The temperature distribution along the length of the heat storage unit is constant, as are the temperature and moisture of the air. Therefore, the initial conditions for the air and the composite material are set as follows:

$$x_{\mathrm{a}} = x_{\mathrm{a,0}}, T_{\mathrm{a}} = T_{\mathrm{a,0}}, T_{\mathrm{s}} = T_{\mathrm{s,0}}, \omega_0 = \omega_{\mathrm{sor/desor}} \qquad \text{at } t = 0 \qquad (18)$$

2.3 Parameter settings

2.3.1 Determination of the equilibrium sorption amount

Two phases of $H_2O$ co-exist, namely, gas and sorbed water inside the pores of the composite medium. The water vapor sorption isotherms of the composite material were tested by the water vapor sorption analyzer Hydrosorb HS-1 (Quantachrome Instruments). At the four measured temperatures (25, 30, 35, 40°C), the equilibrium sorption amount is essentially independent of temperature and only related to the relative humidity, as shown in Fig. 2(a). Therefore, the equilibrium sorption amount $\omega_{\mathrm{e}}$ is assumed to be independent of temperature, and is only a function of relative humidity in the calculation.

$$\omega_{\mathrm{e}} = f(RH) \qquad (19)$$

The water vapor sorption isotherms shown in Fig. 2(a) was tested by heating the material at 150ºC under the vacuum condition for 4 hours to make sure that the material had been dried

completely. However, for WSS + 22.4 wt% $CaCl_2$, the equilibrium sorption amount tends to be nonzero when the relative humidity is small if it is regenerated at 80ºC. This condition is due to the formation of calcium chloride dihydrate, which is verified by Fig. 4 in [2]. Therefore, in order to get a clear idea about the effect of crystalline dehydrate on the equilibrium sorption amount at each relative humidity, the water vapor sorption isotherm was tested again by heating the same material at 80ºC for 4 hours, and the initial sorption amount is nonzero when the relative humidity is small, which can be seen in Fig. 2(b). The equilibrium sorption amount used in the simulation was obtained by the cubic spline interpolating method based on several measured sorption amount values.

2.3.2 Determination of the sorption heat

The sorption/desorption heat for the composite material can be obtained from its sorption characteristics, which is related to the water sorption amount [26]. The sorption heat is high when the sorbed water is smaller than 2 moles per mole of $CaCl_2$ (corresponds to $CaCl_2 \cdot 2H_2O$) then it remains at a constant value [26]. In this simulation, the sorption heat is assumed to be constant and equal to the latent heat of water during the sorption amount range, within which the calcium chloride dihydrate was considered stable during both the sorption process and desorption process.

2.3.3 Overall mass transfer coefficient

The total mass transfer resistance $\frac{1}{K}$ is calculated by adding both resistances in series according to [27]:

$$\frac{1}{K} = \frac{1}{k_a} + \frac{1}{k_s} \tag{20}$$

The air side mass transfer coefficient $k_a$ can be calculated based on the solid side.

$$k_{\mathrm{a}} = \frac{\rho_{\mathrm{a}} h_m}{\rho_{\mathrm{s}} \alpha} \tag{21}$$

The solid side mass transfer coefficient $k_{\mathrm{s}}$ is defined by the following equation according to [20, 28]:

$$k_{\mathrm{s}} = \frac{15 D_s}{\delta_{\mathrm{s}}} \tag{22}$$

2.4 Numerical solution and experimental validation

The governing equations were discretized using the explicit finite difference (FDM) method. The discrete equations were derived over each length interval and time interval and numerically solved by Fortran code.

In this study, experimental results from tests of the open sorption thermal energy storage setup were used to validate the simulation results. The dimensions of the thermal energy storage unit were 20 cm (length) × 10 cm (width) ×10 cm (height). The WSS + 22.4 wt% $CaCl_2$ was chosen for the validation of this program due to its excellent performance in previous experiments, and the simulation conditions are shown in Table 1. The calculated outlet air absolute humidity, change of the sorption amount, outlet air temperature, and the composite material's temperature and corresponding instantaneous sorption amount, as well as the relevant experimental values, are illustrated in Fig. 3(a), (b) and Fig. 4 for the sorption process and in Fig. 5(a), (b) and Fig. 6 for the desorption process, respectively.

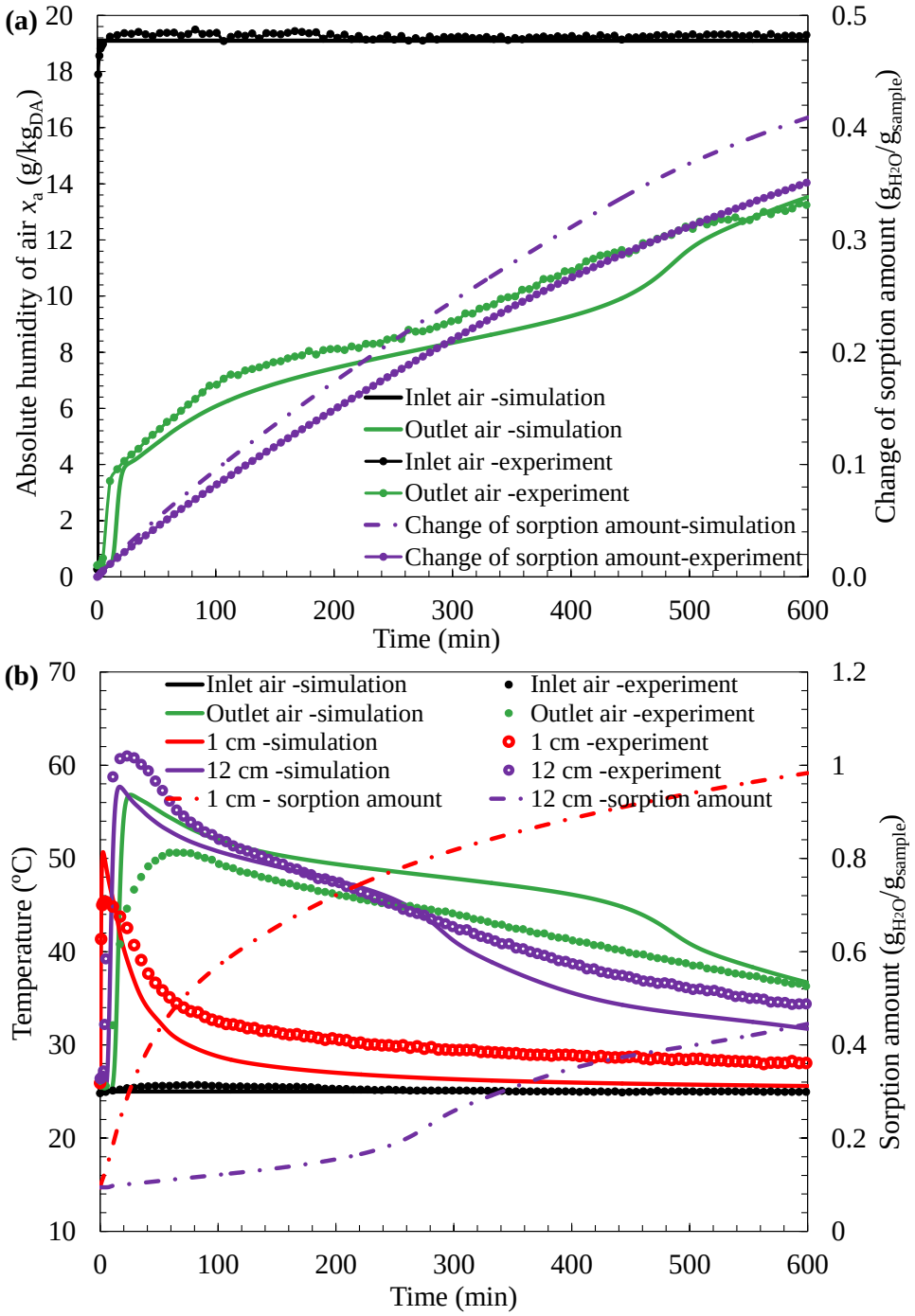


Fig. 3 (a) Comparison of inlet/ outlet air absolute humidity and change of the sorption amount during sorption process; (b) comparison of inlet/outlet air temperature and temperature of the WSS + 22.4 wt% $CaCl_2$ in heat release process (humid air flow rate: 3.0 $m^3$/h; regeneration temperature: 80°C)

Fig. 3(b) and Fig. 4 demonstrate that the simulated composite material's temperatures match the experimental values well both in terms of time and of the position along the length of the WSS + 22.4 wt% $CaCl_2$. The simulation results for the general trend in the outlet air temperature with time are also similar to the experimental results, although the simulated outlet air temperature differs by approximately 3 to 4°C from the measured values (cf. Fig. 3(b)).

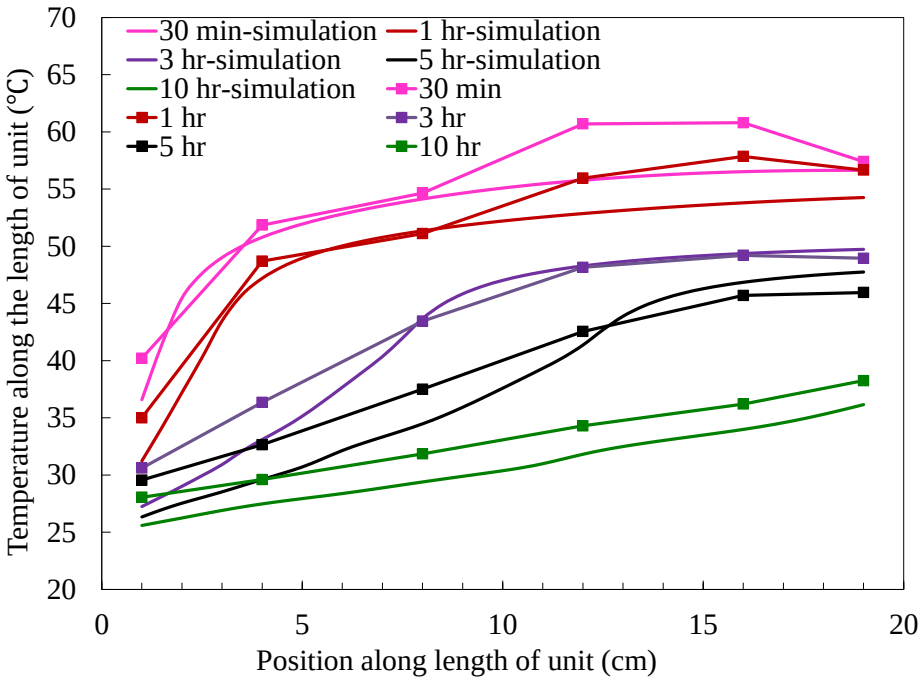


Fig. 4 Temperature profile of the WSS + 22.4 wt% $CaCl_2$ in heat release process (humid air flow rate: 3.0 $m^3$/h; regeneration temperature: 80°C)

The simulated outlet air absolute humidity result shows that more water vapor is sorbed in the simulation than in the experiment, which indicates that more heat was released in the simulation, causing higher outlet air temperatures. This discrepancy is likely due to two major sources. First, the uneven velocity distribution over the cross section of the inlet has an impact on the water vapor sorption amount during the experiment. We measured the temperature and relative humidity at the center of the cross section of the inlet and outlet of

the heat storage unit. The highest sorption behavior (high relative humidity can produce a high sorption amount according to Fig. 2(b)) was calculated according to the measured inlet air relative humidity. Second, according to Fig. 5(b), the measured final temperature (< 80°C) of the latter part of the heat storage unit affects the equilibrium sorption amount in the desorption process. In the simulation, the initial sorption amount in the sorption process is defined as the sorption amount under the local air's relative humidity, which is higher than the actual value for the latter part of the heat storage unit.

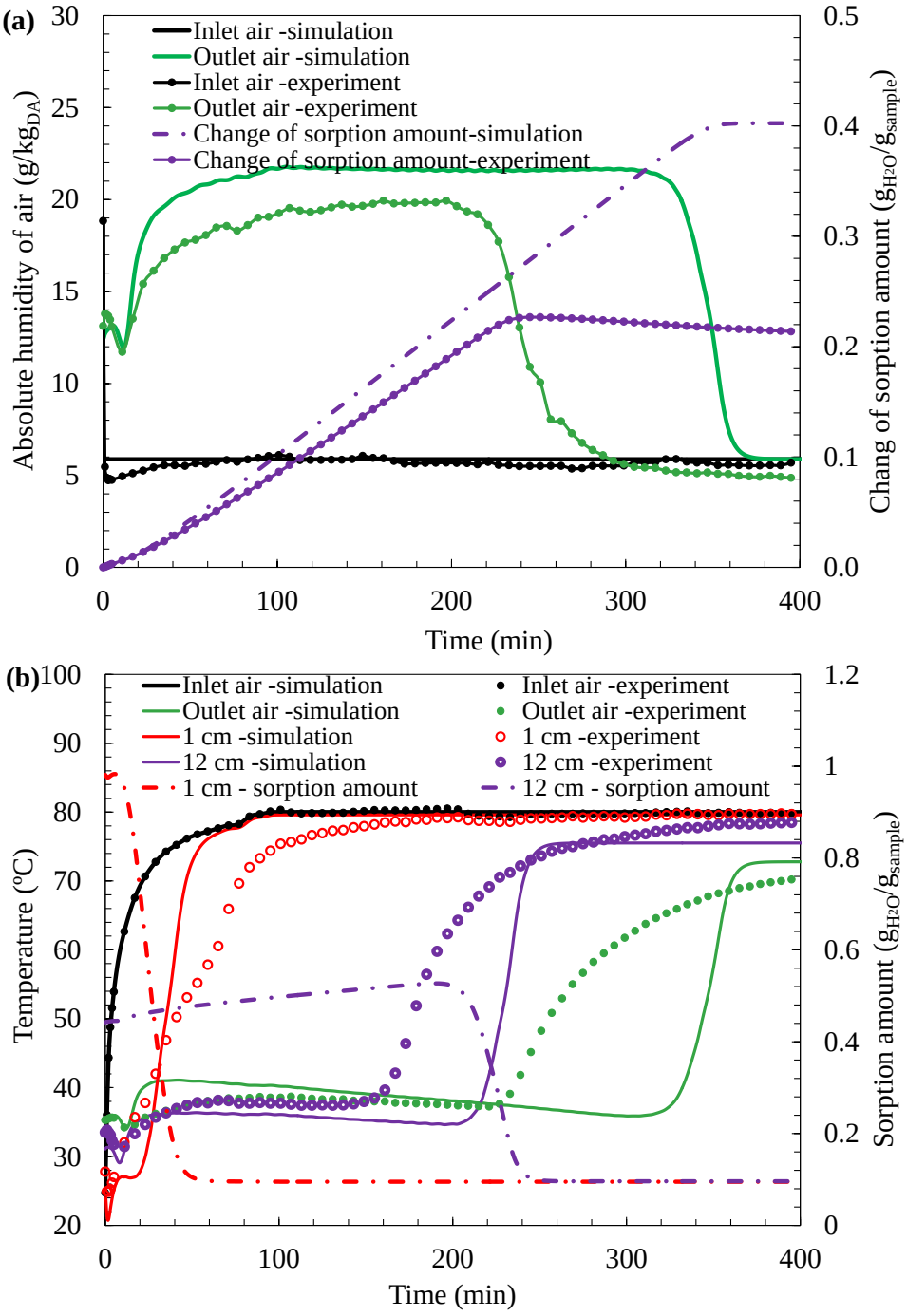


Fig. 5 (a) Comparison of inlet/ outlet air absolute humidity and change of the sorption amount during desorption process; (b) comparison of inlet/outlet air temperature and temperature of the WSS + 22.4 wt% $CaCl_2$ in heat desorption process (hot air flow rate: 3.8 $m^3$/h; regeneration temperature: 80°C)

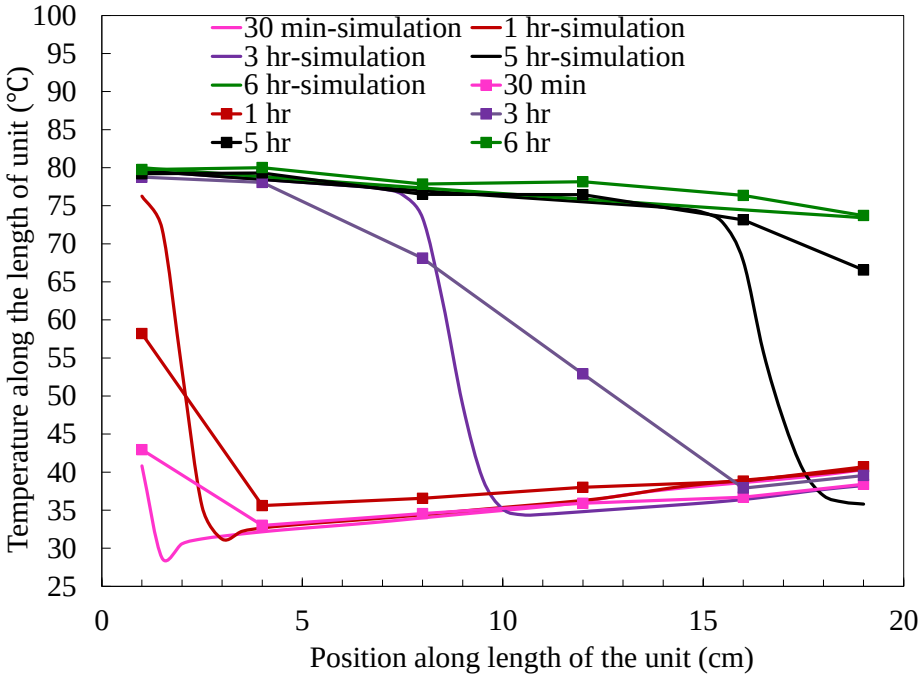


Fig. 6 Temperature profile of the WSS + 22.4 wt% $CaCl_2$ in heat storage process (hot air flow rate: 3.8 $m^3$/h; regeneration temperature: 80°C)

Comparison of the regeneration process results are illustrated in Fig. 5(a), (b) and Fig. 6. The calculated material's temperature, as well as the outlet air temperature and absolute humidity, approximately fit the measured values during the beginning of the desorption process. However, the calculated material's temperature, outlet air temperature, and outlet absolute humidity lag behind the measured values as the desorption process progresses. This discrepancy is mainly caused by (a) the higher calculated sorption amount in the sorption process and (b) the difference in the change of sorption amount between the sorption process (cf. Fig. 3(a)) and the desorption process (cf. Fig. 5(a)) in the experiment. The uneven distribution of velocity over the cross section of the heat storage unit also contributes to this difference. For the sorption process, the velocity of the humid air is lower than that of the hot air in the desorption process. Therefore, the uneven distribution in the relative humidity of the inlet air is more pronounced in the sorption process than in the desorption process.

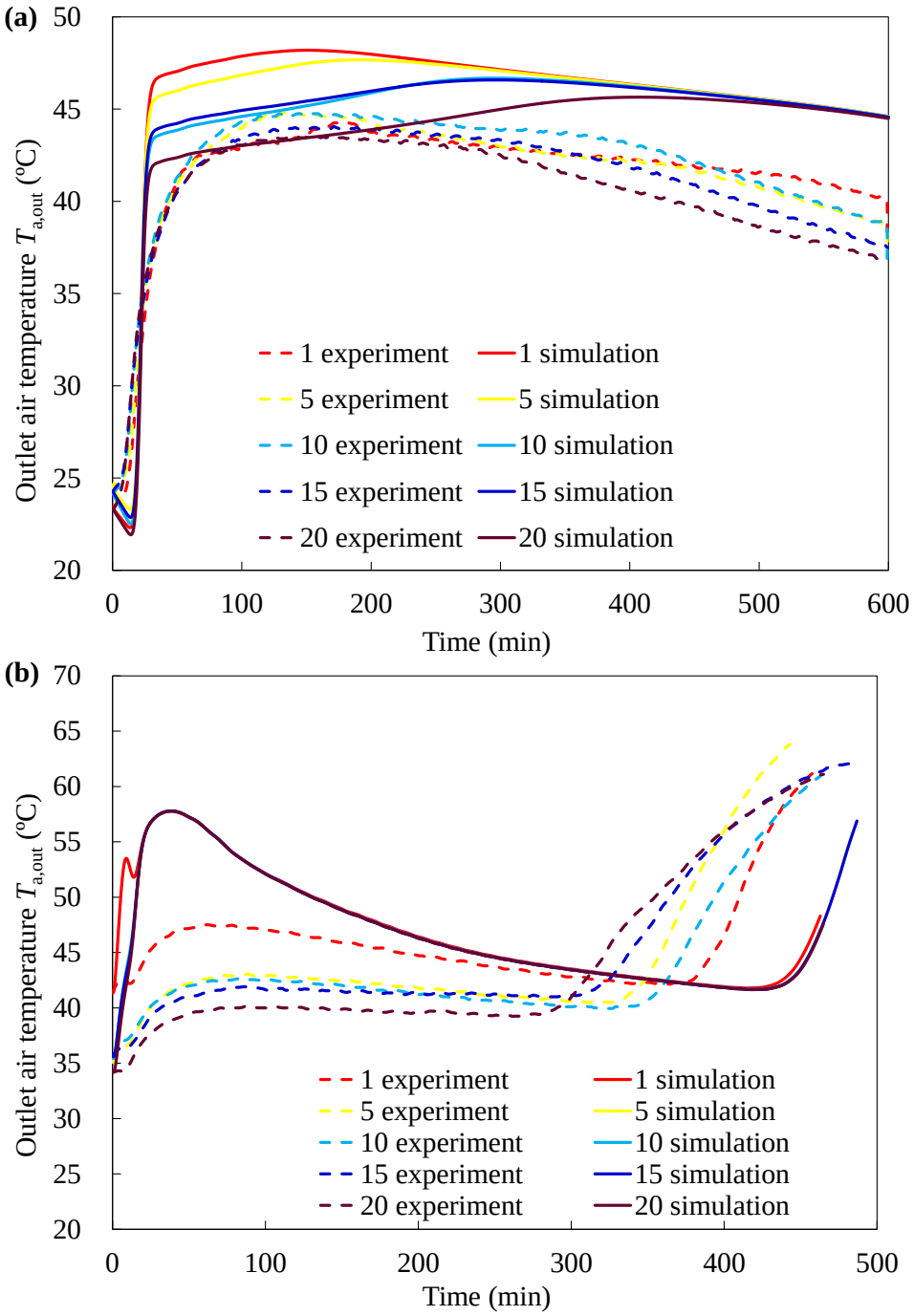


Fig. 7 (a) Comparison of the outlet air temperature during the heat release process; (b) comparison of the outlet temperature during the regeneration process of the WSS + 22.4 wt% $CaCl_2$ (humid air flow rate: 2.0 $m^3$/h; hot air flow rate: 2.8 $m^3$/h; regeneration temperature: 80°C)

Regeneration/sorption processes were simulated 20 times using a humid air flow rate of 2.0 $m^3$/h, an air temperature of 25°C, a hot air flow rate of 2.8 $m^3$/h, and a regeneration temperature of 80°C by inputting the initial conditions repeatedly according to the experimental measurements. The comparison of the simulated outlet air temperature and the experimental results is illustrated in Fig. 7(a) and (b). The simulated outlet air temperature differs only slightly from the measured values in the sorption process in contrast to the larger discrepancy observed for the desorption process. The likely reasons for the discrepancy observed in the desorption process have been explained above. The results of the repeated simulations allow us to ensure that this program can provide a stable performance over many operation times.

## 3. Definitions of performance evaluation indices

Numerical tests of the WSS + 22.4 wt% $CaCl_2$ under various thermal energy storage conditions were performed to test the effect of each key parameter, determine the best practical operating conditions, and evaluate the performance of the open sorption thermal energy storage system.

To evaluate the performance of the thermal energy storage system, we used multiple performance indices. The volumetric heat storage density $Q_V$ (available heat output in the sorption process per $m^3$), the actual total heat output $Q_{sor}$, the maximum potential stored heat $Q_{max}$, and the coefficient and effective coefficient of heat extraction performance $\varepsilon$ and $\varepsilon_{eff}$ in the heat release process were defined as follows:

$$Q_V = C_{p,a}\rho_a f\int_{\Delta t}(T_{a,out} - T_{a,in})dt / V \tag{23}$$

In the above equation, during the time interval $\Delta t$, the temperature difference of outlet air and inlet air $\Delta T$ is no lower than 15ºC.

$$Q_{\mathrm{sor}} = (\Delta\omega)(\Delta H)m_{\mathrm{s,dry}} \tag{24}$$

$$Q_{\max} = (\Delta\omega)_{\max}(\Delta H)m_{\mathrm{s,dry}} \tag{25}$$

$$\varepsilon = (Q_V V)/Q_{\max} \tag{26}$$

$$\varepsilon_{\mathrm{eff}} = (Q_V V)/Q_{\mathrm{sor}} \tag{27}$$

The heat recovery rate $\eta$ of this thermal energy storage system must also be evaluated by incorporating the performance of the regeneration process, which is important when the exhaust heat or renewable energy is limited. The total heat consumed to regenerate the composite material can be calculated from the difference in the inlet and outlet air temperature:

$$Q_{\mathrm{desor}} = C_{p,\mathrm{a}}\rho_{\mathrm{a}} f\int_0^t (T_{\mathrm{a,in}} - T_{\mathrm{a,out}})dt \tag{28}$$

$\eta$ is evaluated as the ratio of the heat released in the sorption process and the heat stored in the desorption process:

$$\eta = Q_{\mathrm{sor}}/Q_{\mathrm{desor}} \tag{29}$$

The effective heat recovery rate $\eta_{\mathrm{eff}}$ is related to the ratio between the effective heat absorbed by the flowing air in the sorption process and the total heat input in the desorption process.

$$\eta_{\mathrm{eff}} = (Q_V V)/Q_{\mathrm{desor}} \tag{30}$$

## 4. Results and Discussion

Because we examined the influence of the filling amount of $CaCl_2$ during the sorption process in our previous work, we focused on the other important parameters in the present study. The input parameters for each section are listed in Table 2.

**Table 2** Calculation conditions

| Key parameters | Inlet air temperature (°C) | Inlet air relative humidity (%) | Humid air flow rate ($m^3$/h) | Length of filter (cm) |
|---|---|---|---|---|
| Section 4.1 | 15<br>20<br>25<br>30 | 95 | 3.0 | 20 |
| Section 4.2 | 25 | 65<br>75<br>85<br>95 | 3.0 | 20 |
| Section 4.3 | 25 | 95 | 3.0<br>4.0<br>5.0<br>6.0 | 20 |
| Section 4.4 | 25 | 95 | 3.0 | 10<br>15<br>20<br>25 |

4.1 Influence of the inlet air temperature

The dynamic variations of the relative humidity and temperature of the outlet air and the temperature difference between the inlet and outlet air are shown in Fig. 8. Here, the material's initial temperature is the same as the given inlet air temperature in the sorption process. The relative humidity of the inlet air was kept at 95% for all four inlet air temperatures. Because the composite material was very dry at the initiation of the sorption process, the outlet air was dehumidified in this process. Fig. 8 also illustrates that the outlet air's relative humidity rises when the inlet air temperature is high. This process is thought to occur because high temperature causes high water vapor content (high absolute humidity) in the flowing air. The system cannot discharge heated air with a high outlet and inlet temperature difference for long when the inlet air temperature is high during the heat discharging process.

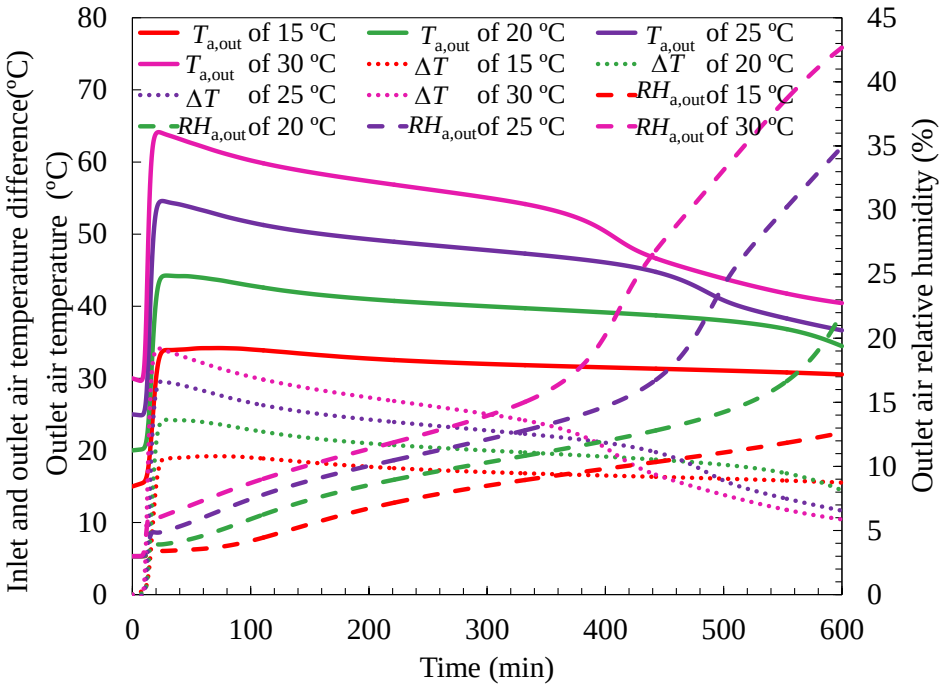


Fig. 8 Outlet air relative humidity, outlet air temperature and outlet and inlet air temperature difference change with time of different inlet air temperatures

4.2 Effect of the inlet air relative humidity

As shown in Fig. 9, the duration of the discharge of high-temperature outlet air is prolonged when the relative humidity increases. Indeed, the equilibrium sorption amount also increases with higher relative humidity according to the isothermal equilibrium sorption amount line shown in Fig. 2(b). It is notable that the water vapor content of the inlet air has an important impact on the outlet air temperature during the heat release process due to the high sorption amount at high relative humidity. The relative humidity of the inlet air is an important parameter for the optimal performance of the thermal energy storage unit.

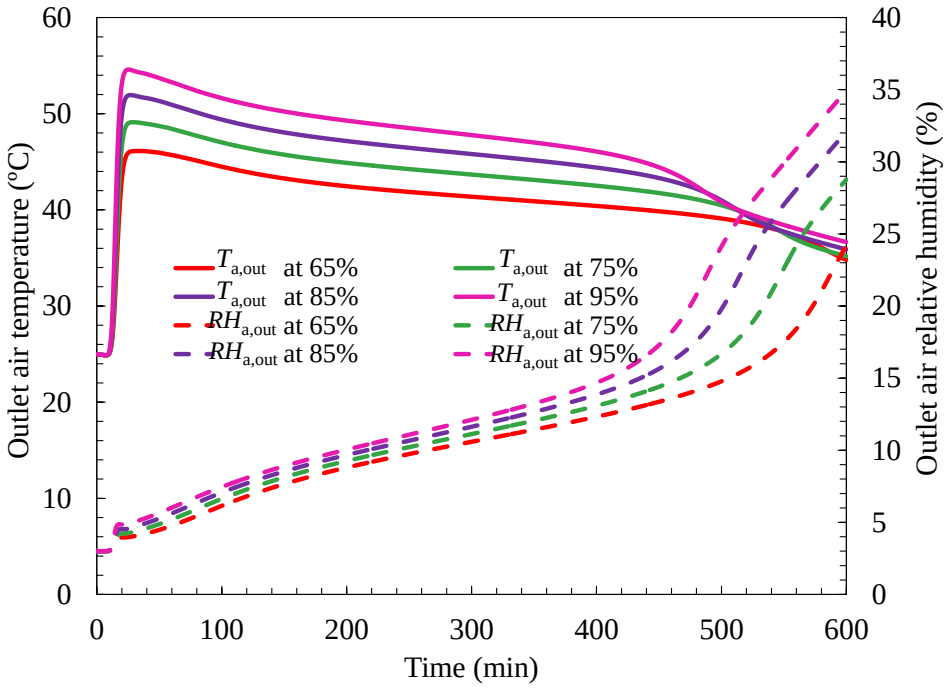


Fig. 9 Outlet air relative humidity and outlet air temperature change with time of different inlet air relative humidies

4.3 Influence of the humid air flow rate

Fig. 10 shows that the outlet air's relative humidity increases with the humid air's flow rate, an effect caused by the relationship between the sorption rate and the supplied mass flow of water vapor. The discharge duration of the high-temperature outlet air decreases when the air flow rate is high, as more heat is released per time with a faster flow. Additionally, the rate of outlet air temperature increase grows greater with increasing air flow rate. The same phenomenon was found in our previous experiment [2], and we believe this effect is due to thinning of the air film near each channel's surface, which causes the water vapor diffusion rate to increase due to lower gas film resistance. More water vapor could thus diffuse to the composite material and be sorbed while simultaneously generating more heat.

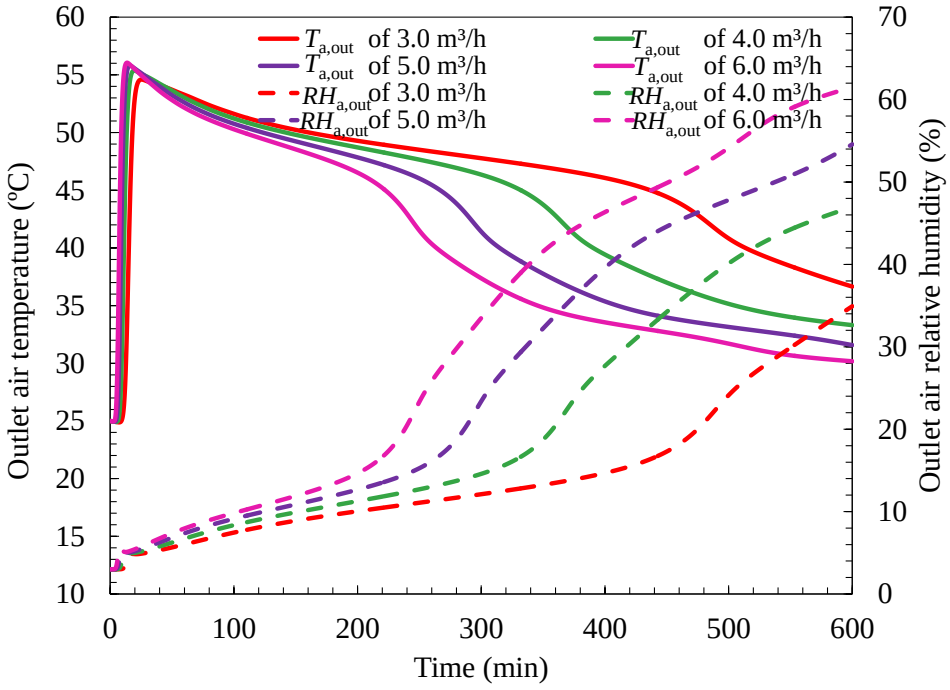


Fig. 10 Outlet air relative humidity and outlet air temperature change with time of different humid air flow rates

4.4 Influence of the length of the thermal energy storage unit

The performance of the WSS + 22.4 wt% $CaCl_2$ with a length of 10 cm is compared with the experimental results illustrated in Fig. 11(a) and (b). The simulated outlet air absolute humidity and the temperature of the material approximately fit the measured values, indicating that our simulation can be applied to predict the behavior of thermal energy storage units with different lengths. The results for various lengths are shown in Fig. 12. Increasing the length of the heat storage unit increases the contact time between the flowing air and each channel. A longer one thus leads to a longer-duration discharge of high-temperature outlet air. However, the maximum outlet temperature of the longer one is not significantly higher than that of the shorter one.

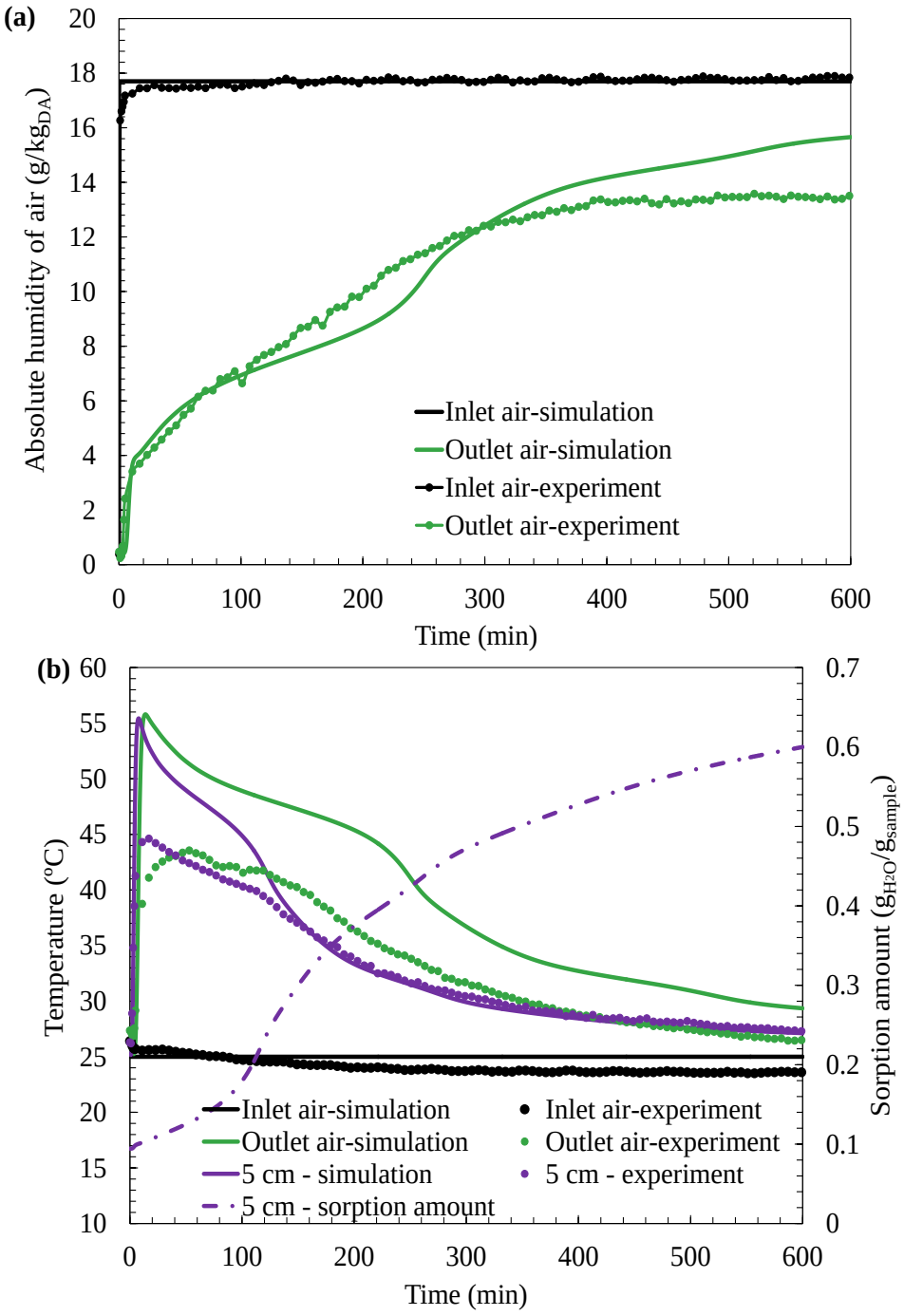


Fig. 11 (a) Comparison of inlet and outlet air absolute humidity; (b) comparison of inlet/outlet air temperature and temperature of the WSS + 22.4 wt% $CaCl_2$ with a length of 10 cm in heat release process (humid air flow rate: 3.0 $m^3$/h; regeneration temperature: 80°C)

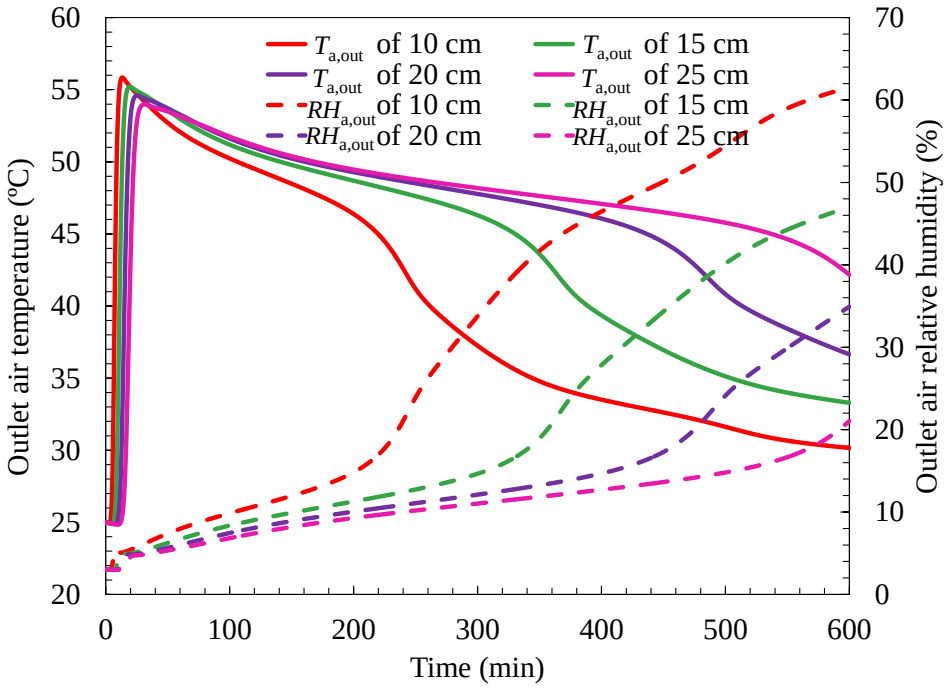


Fig. 12 Outlet air relative humidity and outlet air temperature change with time of different length of the thermal energy storage units

4.5 Comprehensive evaluation of the mass flow of water vapor in the humid air

Inlet air temperature, relative humidity, and flow rate all influence the same parameter, mass flow of water vapor $X_a$, defined by the equation $X_a = \rho_a f x_{a,in}$. The effect of the mass flow of water vapor can be seen in Fig. 13(a) and (b). When more water vapor is supplied, more water vapor can be sorbed, releasing more heat (cf. Fig. 13(a)). Moreover, with higher amounts of supplied water vapor, the effective heat that can be utilized per unit volume will be higher. For a given humid air flow rate, the higher the mass flow of water vapor, the better the performance, with heat released and volumetric heat storage density both increasing with the mass flow of water vapor.

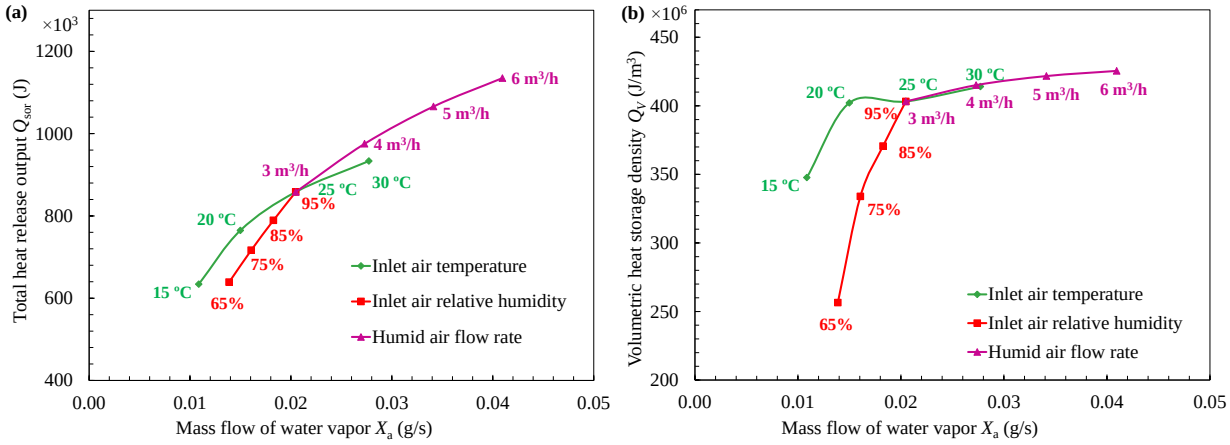


Fig. 13 (a) Effect of absolute water vapor content on total heat release amount; (b) effect of absolute water vapor content on volumetric heat storage density

4.6 Evaluation of each key parameter of the thermal energy storage system

The effects of each parameter have been evaluated by calculating the effective coefficient of heat extraction $\varepsilon_{\text{eff}}$ and the volumetric heat storage density $Q_V$ (shown in Fig. 14(a), (b), and (c)), the total heat release amount $Q_{\text{sor}}$ and the coefficient of heat extraction $\varepsilon$ (shown in Fig. 15(a) and (b)), and $\eta$ and $\eta_{\text{eff}}$ (shown in Fig. 16(a) and (b)). In the simulation, the hot air's temperature is 80°C, with a flow rate of 3.8 $m^3$/h during the regeneration process. When calculating all the evaluation indices, the simulation time of the sorption process was kept constant at ten hours, but for some cases, the simulation was repeated with a different operating time to further explore certain phenomena.

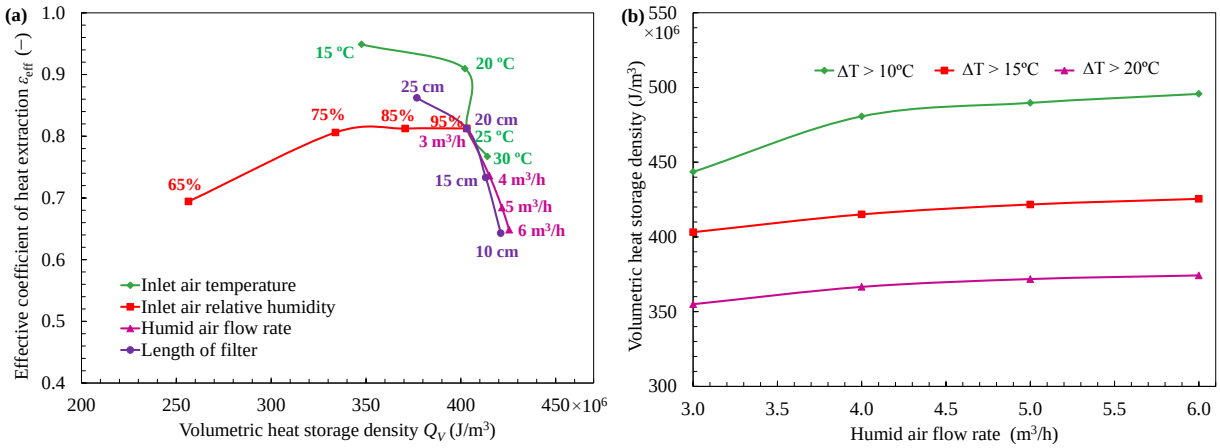


Fig. 14 (a) Effect of each parameter on volumetric heat storage density and effective coefficient of heat extraction during heat release process; (b) effect of inlet and outlet air temperature difference on volumetric heat storage density; (c) effect of heat release duration on volumetric heat storage density

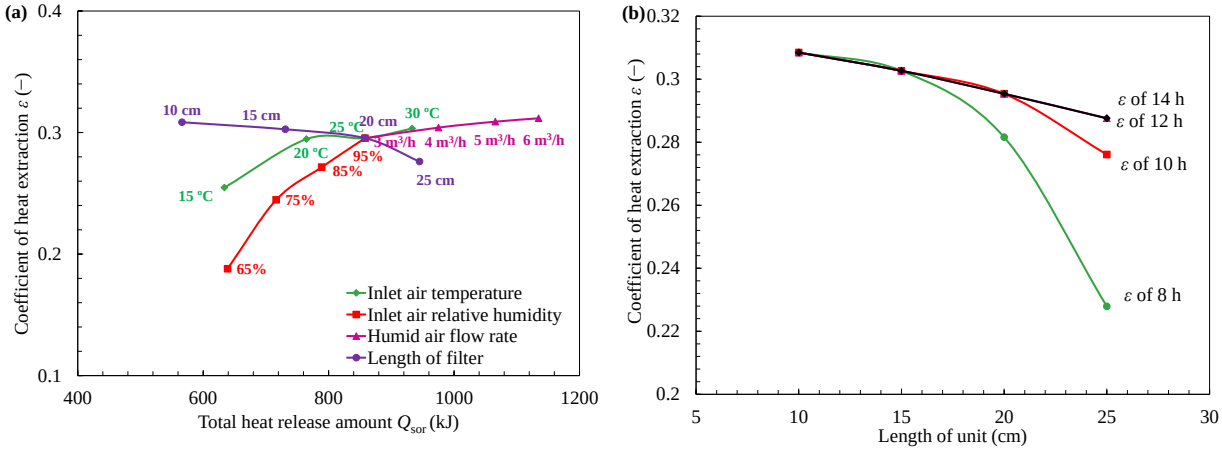


Fig. 15 (a) Effect of each parameter on total heat release amount and coefficient of heat extraction during heat release process; (b) effect of heat release duration on coefficient of heat extraction

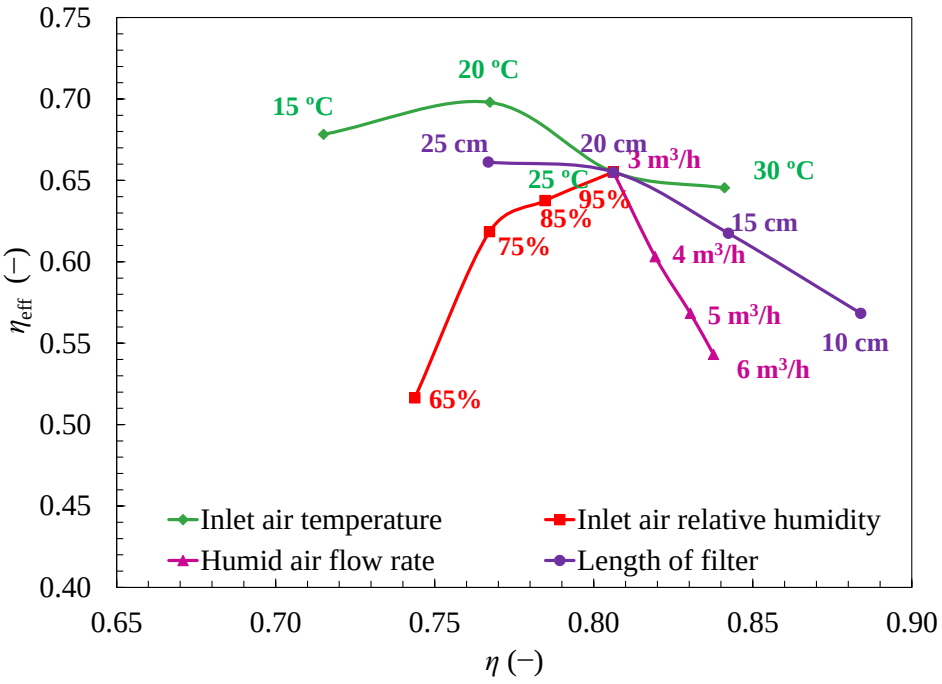


Fig. 16 Effect of each parameter on $\eta$ and $\eta_{eff}$ of the open sorption thermal energy storage system

Fig. 14(a) demonstrates that because of the high mass flow of water vapor in the air, high inlet air relative humidity, and high inlet air temperature, our system could exhibit a high volumetric heat storage density. For different operating requirements for air temperature, the humid air flow rate shows an important effect on the volumetric heat storage density. If the required temperature is lower than 35°C, the lowest volumetric heat storage density occurs when the flow rate is 3.0 $m^3$/h, as shown in Fig. 14(b). However, under other requirements, the flow rate does not affect the volumetric heat storage density.

Within ten hours, the shortest thermal energy storage unit shows the highest volumetric heat storage density; however, for a different desired operating time, another length may be better (cf. Fig. 14(c)). A longer honeycomb thermal energy storage unit can supply almost the same amount of effective heat per volume.

The effective coefficient of heat extraction increases when the inlet air relative humidity or the length of the heat storage unit rises or when the humid air flow rate decreases. When the relative humidity is maximized, the humid air flow rate is 3 $m^3$/h and the inlet air temperature is kept at 20 to 30ºC, the system achieves a high volumetric heat storage density, as well as a high $\varepsilon_{eff}$, as illustrated in Fig. 14(a).

When high mass flow of water vapor is supplied (cf. Fig. 13(a)), the resulting inlet air relative humidity, inlet air temperature, and speed of the humid air can produce a high total heat release amount. According to Fig. 15(a), if the heat release time is within ten hours, the heat storage unit's length is shorter than 25 cm and shows almost the same coefficient of heat extraction. However, if hot air is needed for duration longer than ten hours, a longer one provides a better performance compared to cases where hot air is provided for a shorter time due to its higher sorption ability, as illustrated in Fig. 15(b).

When the exhaust heat or renewable heat to be stored is limited, the heat recovery rate $\eta$ and effective heat recovery rate $\eta_{eff}$ must be considered to evaluate the whole cycle's performance. Fig. 16 indicates that, due to the effect of the mass flow of water vapor, high inlet air temperature, high relative humidity, and a large air low rate produce a high heat recovery rate, while a shorter one can achieve a high $\eta$ due to the high sorption amount of the whole thermal energy storage unit. However, a longer one can provide a better $\eta_{eff}$ for a release duration of ten hours due to its high $\varepsilon_{eff}$.

Based on the above analysis, the optimal operating conditions for ten hours of heat release are as follows: $T_{a,in}$ = 25°C or 30°C, $RH_{a,in}$ = 95%, $f_a$ = 3.0 $m^3$/h, $L$ = 20 cm or 25 cm to get a high volumetric heat storage density $Q_V$, a high effective coefficient of heat extraction $\varepsilon_{eff}$ and a high effective heat recovery rate $\eta_{eff}$. If a longer-duration heat release is required, a longer thermal energy storage unit is necessary.

4.7 Simulation of an application of the open thermal heat storage system

In this section, the thermal energy storage system is applied to a paint-drying system. When thick coats of paint are needed for large pumps, the hot ventilated air required for paint drying is usually supplied by a kerosene-fueled blower during the daytime. Ventilation with natural outdoor air is generally used during the nighttime (cf. Fig. 17(a)). Speeding up the drying process while minimizing the cost is an important challenge. One solution is to run the kerosene-fueled blowers in the nighttime as well as during the day, but doing so requires watchmen and is thus costly. Therefore, we propose the incorporation of our open sorption thermal energy storage unit into this system. The exhaust heat from the kerosene-fueled blowers employed during the daytime can be stored using the thermal energy storage unit. The stored heat can be utilized to heat up ventilated air, which can be employed in the drying booth during the nighttime as shown in Fig. 17(b). Another advantage of this system is the low relative humidity of the supply air from the thermal energy storage unit. Our system can simultaneously shorten the drying process and save energy.

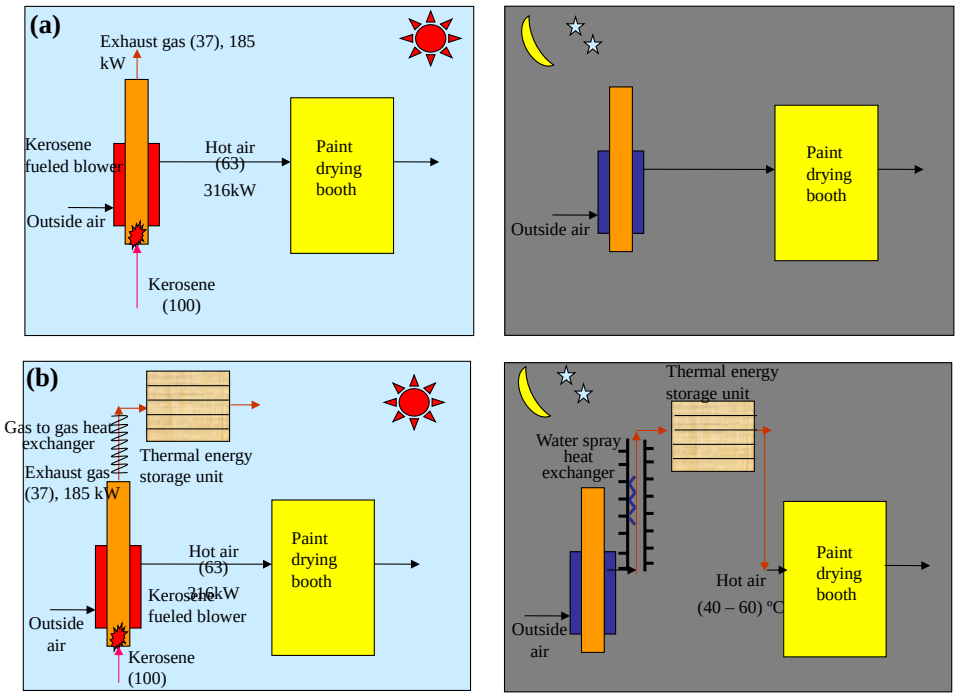


Fig. 17 (a) Previous paint drying system; (b) improved system incorporated with the

developed sorption thermal energy storage unit

In our proposed application, the hot air needed for regenerating the composite material is supplied by the heated exhaust from the blower. The operating conditions of the thermal energy storage system are shown in Table 3. During the daytime, the kerosene fuel blower with efficiency of 63% is used to dry the paint drying booth. While an air to gas heat exchanger is assumed to exchange heat with the exhaust gas from the kerosene boiler to regenerate the thermal energy storage unit. For the nighttime operation, a spray heat exchanger with fins outside is assumed to be used to increase the relative humidity of the flowing air, which is necessary for the thermal energy storage unit to supply high temperature air in the nighttime. In fact, the spray heat exchanger is a humidifier with high heat exchanger rate to increase the inlet air temperature by absorbing heat from the indoor air at the same time.

**Table 3** Application condition for designing the thermal energy storage unit

| | Parameters | Value |
|---|---|---|
| Kerosene boiler | Heat output | 500 kW |
| | Combustion gas temperature | 200°C |
| | Operation time duration | 8:00-18:00 |
| Kerosene fuel blower | Efficiency | 63% |
| | Exchanged gas's temperature | >100°C |
| Gas to gas heat exchanger | Efficiency | 80% |
| | Air's temperature | (80-85)°C |

The proposed system was designed to be able to supply hot air in the nighttime for at least 14 hours. Wet air with a relative humidity of 95% was selected because of its effectiveness in all evaluation indices. Because of the natural outdoor air temperature and the indoor air temperature, an inlet humid air temperature of 25°C was selected. A humid air flow rate of

3.0 $m^3$/h was chosen to ensure a sufficient duration of hot air release, as illustrated in Fig. 10, and high $\varepsilon_{eff}$ and $\eta_{eff}$, as shown in Fig. 14(a) and Fig. 16, respectively. According to Fig. 14(c), when the air flow rate is 3 $m^3$/h, the 25 cm thermal energy storage unit achieves the same available heat for operating times of 12 hours and 14 hours, indicating that the maximum available heat can be reached within 12 hours for this thermal energy storage unit length. For the proposed application, a longer one of at least 33 cm was used to supply air at temperatures greater than 40°C for 14 hours.

For the heat storage process, hot air from the gas-to-gas heat exchanger flows through the heat storage unit for ten hours to regenerate it. The flow rate of the hot air through each thermal energy storage unit was set to at least 3.8 $m^3$/h in order to be regenerated completely within ten hours. If the simulated results fulfilled the requirements of the drying system, the size of the heat storage unit was then decided according to the exhaust heat supply side and the performance of the storage unit.

Fig. 18 shows the outlet air temperature and relative humidity trends during the sorption and desorption processes. According to our simulation, the hot air (temperature greater than 40°C) generated by the thermal energy storage unit can dry the painting booth for 14 hours with low relative humidity in nighttime. The exhaust heat produced during the daytime operation of the blowers can also regenerate the heat storage unit successfully.

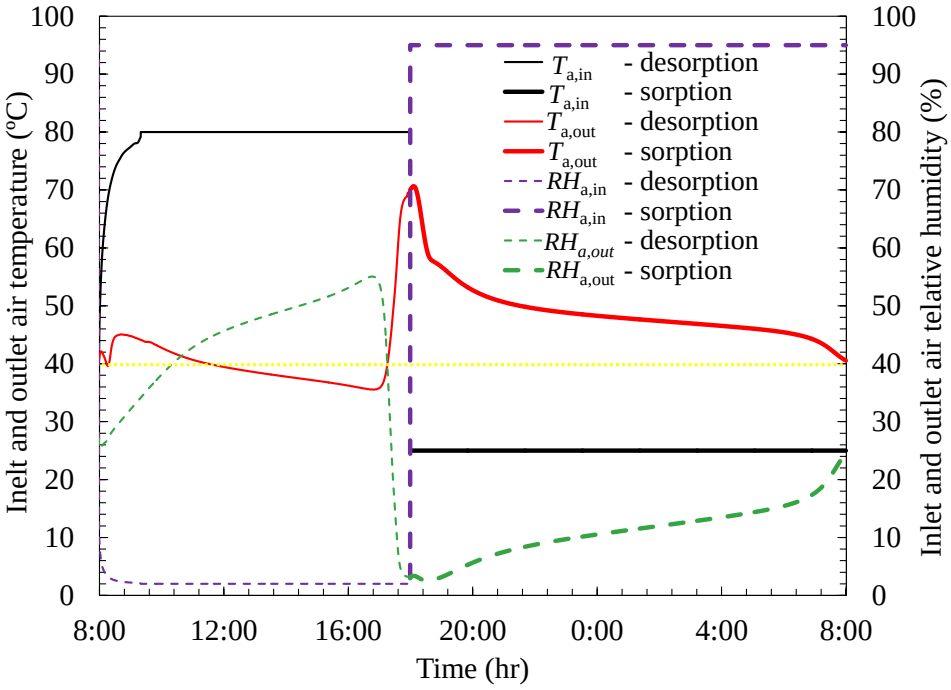


Fig. 18 Simulated outlet air relative humidity and outlet air temperature during the sorption and desorption processes, respectively

The volumetric heat transfer rate, a key parameter defined in Eq. (31), effectively determines the size of the thermal energy storage system, as is shown in Fig. 19.

$$W_V = C_{p,a}\rho_a f \left|T_{a,out} - T_{a,in}\right| / V \tag{31}$$

From the value of the desorption volumetric heat transfer rate and the exhaust heat amount, the necessary volume of the thermal energy storage unit was determined to be 7.7 $m^3$, which means that at least 2300 thermal energy storage unit with dimensions: 10 cm (width) ×10 cm (height) ×33 cm (length) are necessary.

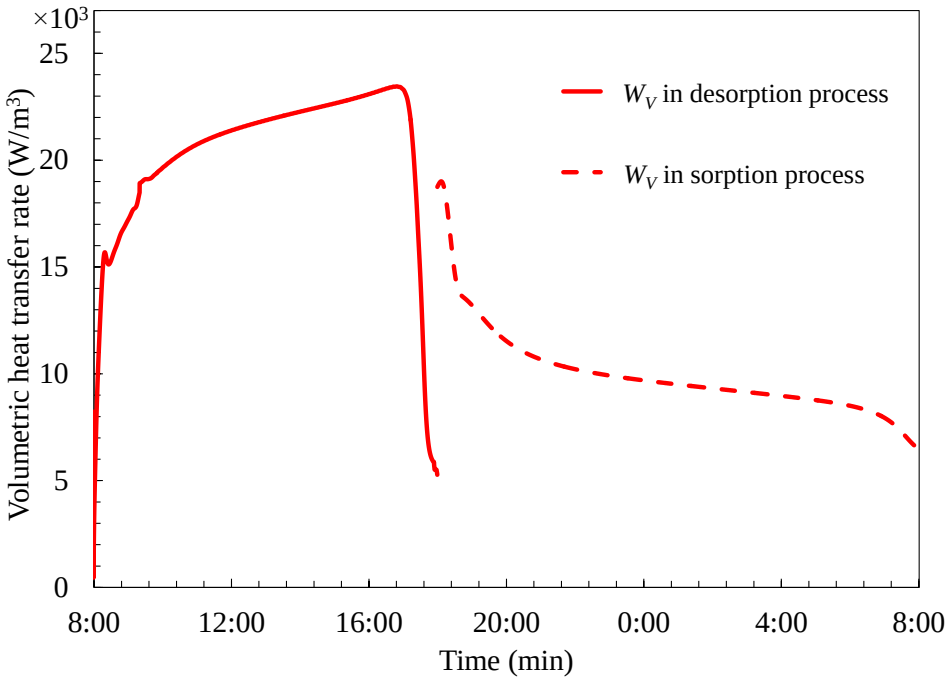


Fig. 19 Volumetric heat transfer rate of the open thermal energy storage unit

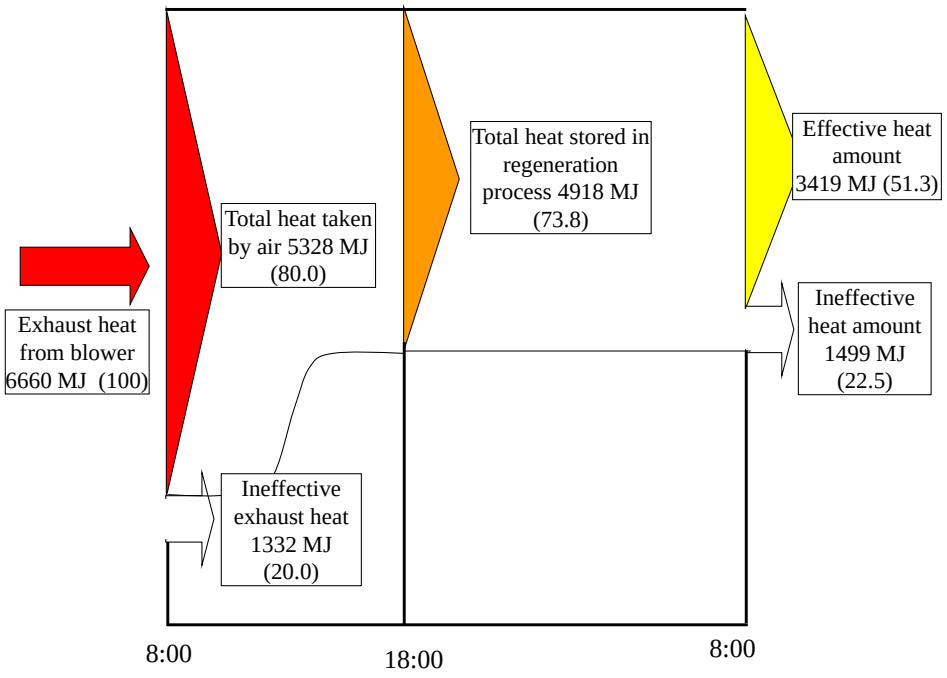


Fig. 20 Energy flow chart of the improved paint drying system incorporated with the open thermal energy storage unit

The energy flow chart for this application shown in Fig. 20 was studied to investigate the efficiency of the thermal energy storage system in the drying process. The total exhaust heat generated by the blower is 6660 MJ within its operation time, and a fraction of this heat (4918 MJ) must be utilized to regenerate the thermal energy storage unit in the daytime. The effective heat needed to dry the paint-film is approximately 3419 MJ at nighttime, which is approximately 51.3% of the total exhaust heat. Thus, the thermal energy storage unit can recover half of the exhaust heat and improve the dryness quality (keeping proper temperature and low relative humidity of supplied air) of the paint-film.

## 5. Conclusions

A numerical simulation model was created to investigate the capability of a composite mesoporous thermal energy storage unit to store thermochemical energy. This program, based on the effect of coupled heat and mass transfer, effectively simulates our open sorption thermal energy storage system. From the numerical results, we obtained the following conclusions:

1. The simulation results can approximately predict the experimental values. The discrepancies observed between simulation and experiment in the desorption process have been explained above.

2. Using our simulation program, we analyzed the effects of the inlet air temperature and relative humidity, humid air flow rate, and thermal energy storage unit length on the system's performance. Optimal operating conditions were thus selected as follows: $T_{a,in}$ = 25°C or 30°C, $RH_{a,in}$ = 95%, $f_a$ = 3.0 $m^3$/h, $L$ = 20 or 25 cm for a heat release duration of ten hours.

3. A realistic application was proposed and simulated. Based on the simulation results, the thermal energy storage unit can supply air with a temperature greater than 40°C for 14 hours, and the unit can be regenerated within ten hours during the daytime. Finally, 51.3% of the

exhaust heat generated by a kerosene-fueled blower can be recovered using the thermal energy storage unit, and the dryness quality level of the paint-film can be improved.

**Acknowledgements**

The authors would like to thank Dr. Togawa and Dr. Nabeshima, researchers from Hokkaido University, and Mr. Sugiyama, a master's student, for their help with both experiments and simulations. Financial support from the Ministry of Education, Culture, Sports, Science and Technology in Japan is greatly appreciated.

**References**

[1] I. Dincer, Thermal energy storage systems as a key technology in energy conservation, International Journal of Energy Research 26 (2002) 567-588.

[2] H. Liu, K. Nagano, D. Sugiyama, J. Togawa, M. Nakamura, Honeycomb filters made from mesoporous composite material for an open sorption thermal energy storage system to store low-temperature industrial waste heat, International Journal of Heat and Mass Transfer 65 (2013) 471-480.

[3] G. Balasubramanian, M. Ghommem, M.R. Hajj, W.P. Wong, J.A. Tomlin, I.K. Puri, Modeling of thermochemical energy storage by salt hydrates, International Journal of Heat and Mass Transfer 53 (2010) 5700-5706.

[4] D. Zhu, H. Wu, S. Wang, Experimental study on composite silica gel supported CaCl2 sorbent for low grade heat storage, International Journal of Thermal Sciences 45 (2006) 804-813.

[5] H. Wu, S. Wang, D. Zhu, Effects of impregnating variables on dynamic sorption characteristics and storage properties of composite sorbent for solar heat storage, Solar Energy (2007) 864-871.

[6] H. Wu, S. Wang, D. Zhu, Y. Ding, Numerical analysis and evaluation of an open-type thermal storage system using composite sorbents, International Journal of Heat and Mass Transfer 52 (2009) 5262-5265.

[7] N.M. Ostrovskii, N.A. Chumakova, N.M. Bukhavtsova, N.V. Vernikovskaya, Y.I. Aristov, Effect of capillary condensation on water sorption by composite calcium chloride in a porous matrix sorbents, Theoretical Foundations of Chemical Engineering 41(2) (2007) 200-204.

[8] N.M. Ostrovskii, N.A. Chumakova, N.M. Bukhavtsova, N.V. Vernikovskaya, Y.I. Aristov., Modeling of the limiting step of Water Sorption by Composite Sorbents of the

"Calcium Chloride in Porous Matrix" Type, Theoretical Foundations of Chemical Engineering 41(1) (2007) 83-90.

[9] J.L. Niu, L.Z. Zhang, Effects of wall thickness on the heat and moisture transfers in desiccant wheels for air dehumidification and enthalpy recovery, International Communications in Heat and Mass Transfer 29(2) (2002) 255-268.

[10] D. Charoensuphya, W.M. Worek, Parametric study of an open-cycle adiabatic, solid, desiccant cooling system, Energy 13(9) (1988) 739-747.

[11] W. Zheng, W.M. Worek, Numerical simulation of combined heat and mass transfer processes in a rotary dehumifier, Numerical Heat Transfer, Part A: Applications 23(2) (1993) 211-232.

[12] W. Zheng, W.M. Worek, D. Novosel, Performance optimization of rotary dehumidifiers, Journal of Solar Energy Engineering 117 (1995) 40-44.

[13] X.J. Zhang, Y.J. Dai, R.Z. Wang, A simulation study of heat and mass transfer in a honeycombed rotary desiccant dehumidifer, Applied Thermal Engineering 23 (2003) 989-1003.

[14] P. Majumdar, Heat an mass transfer in composite desiccant pore structure for dehumidification, Solar Energy 97(1) (1998) 1-10.

[15] T.S. Ge, F. Ziegler, R.Z. Wang, A mathematical model for predicting the performance of a compound desiccant wheel (A model ofcompound desiccant model), Applied Thermal Engineering 30 (2010) 1005-1015.

[16] Z. Gao, V.C. Mei, J.J. Tomlinson, Theoretical analysis of dehumidification process in a desiccant wheel, Heat Mass Transfer 41 (2005) 1033-1042.

[17] L.Z. Zhang, J.L. Niu, Performance comparisons of desiccant wheels for air dehumidification and enthalpy recovery, Applied Thermal Engineering 22 (2002) 1347-1367.

[18] S. Yamaguchi, K. Saito, Numerical and experimental performance analysis of rotary desiccant wheels, International Journal of Heat and Mass Transfer 60 (2013) 51-60.

[19] A.G. Fedorov, R. Viskanta, Analysis of transient heat/mass transfer and adsorption/desorption internations, International Journal of Heat and Mass Transfer 42 (1999) 803-819.

[20] M. Suzuki, Adsorption engineering. Japan, Kodansya Ltd., Tokyo and Elsevier Science Publishers B. V., Amsterdam, 1990.

[21] C.Q. Zhai, Performance modeling of desiccant wheel design and operation, Doctor degree, Carnegie Mellon University, 2008.

[22] H.H. Xing, Desiccant Dehumidification Analysis, Master Thesis Master of Science in Building Technology, Massachusetts Institute of Technology, 2000.

[23] Y.A. Cengel, Heat Transfer: A Practical Approach, second ed., McGraw-Hill, 2003, pp. 759.

[24] J. Karger, D. M.Ruthven, D. N.Theodorou, Diffusion in Nanoporous Materials, 2 Volume Set. 2012, pp. 85-108.

[25] K.J. Sladek, E.R. Gilliland, R.F. Baddour, Diffusion on surface. 2. Correlation of diffusivities of physically and chemically adsorbed species, Industrial and Engineering Chemistry Fundamentals 13(2) (1974) 100-105.

[26] Y.I. Aristov, M.M.Tokarev, G.Cacciola, G. Restuccia, Selective water sorbents for multiple applications, 1. CaCl2 confined in mesopores of silica gel: sorption properties, Reaction Kinetics and Catalysis Letters 59(2) (1996) 325-333.

[27] T. Tsujiguchi, A. Kodama, Optimum operating/design concept for adsorbent desiccant wheel, Porceeding of Japan Society of Refregerating and Air Conditioning Engineers, Sapporo, Japan, 2012, pp. 107-118.

[28] A. Sakoda, M. Suzuki, Fundamental study on solar powered adsorption cooling system, Journal of Chemical Engineering of Japan 17(1) (1984) 52-57.